EXPERIMENTAL STUDY ON THE DISTRIBUTION PATTERN OF THRESHED AND SEPARATED MIXTURE FOR AN AXIAL-FLOW THRESHING DEVICE WITH ADJUSTABLE THRESHING FORCE

/

脱粒力度可调式纵轴流脱粒装置脱出物分布规律试验研究

Yuejiang TENG[1,2], Chengqian JIN[*3], Fuxiang XIE[1,2], Jian SONG[1,2]

[1] College of Machinery and Automation, Weifang University, Weifang / China;

[2] Shandong Key Laboratory of Intelligent Manufacturing Technology for Advanced Power Equipment, Weifang / China;

[3] Nanjing Institute of Agricultural Mechanization, Ministry of Agriculture and Rural Affairs, Nanjing / China

Tel: +86-19525369138; E-mail: tyj2021to2026@163.com

Correspondent author: Chengqian JIN

DOI: https://doi.org/10.35633/inmateh-78-106

Keywords: *threshing device, adjustable threshing force, threshed and separated material, distribution pattern*

ABSTRACT

To investigate the distribution characteristics of the threshed mixture, threshing and separation experiments were conducted using a self-developed longitudinal axial-flow threshing device with adjustable threshing force, with the adjustable threshing force plates set to the closed mode. The variation patterns of the threshed mixture, grains, stalks, and light impurities along both the axial and radial directions of the threshing drum were obtained experimentally. Based on the experimental data, distribution models of the threshed and separated mixture along the axial and radial directions of the drum were established. The results show that the mass of the threshed mixture beneath the drum accounts for 91.99% of the total feed rate, while the discharged material at the drum outlet accounts for 8.01%. Within the threshed mixture beneath the drum, wheat grains, stalks, and light impurities account for 61.48%, 26.22%, and 12.30% of the total mass, respectively. Based on these findings, the structure of the threshing device was optimized. In the axial range of 1020 ~ 1700 mm along the threshing drum, the grain crushing rate was reduced from 1.16 ~ 12.5% to 1.05 ~ 7.5%. These results provide a theoretical basis and technical reference for the structural design and parameter optimization of threshing, separation, and cleaning systems, contributing to reduced energy consumption and improved operational performance.

摘要

为了研究脱出物的分布规律，在自行研制的脱粒力度可调式纵轴流脱粒装置上进行了脱粒力度调节板处于关闭状态下的脱粒分离试验。通过试验获得脱出物总体、籽粒、茎秆及轻质杂余沿滚筒轴向和径向的变化规律。通过分析获得脱出物沿滚筒轴向和径向的分布规律方程。试验结果表明，滚筒下方脱出物的质量占总喂入量的 91.99%，滚筒尾部排出物的质量占总喂入量的 8.01%。在滚筒下方的脱出物中，籽粒、茎秆及轻质杂余分别占脱出物总质量的 61.48%、26.22%、12.3%。基于试验结果对脱粒装置进行了结构优化，在脱粒滚筒轴向距离 1020mm ~ 1700mm 范围内，籽粒破碎率从 1.16% ~ 12.5%降为 1.05% ~ 7.5%。该试验结果可为脱粒、分离及清选装置的结构设计和参数优化提供参考和依据，从而降低脱粒、分离及清选能耗，提高作业质量。

INTRODUCTION

When the grain harvesting machinery is working, the threshed and separated mixture separated from the concave plate sieve will fall onto the cleaning screen below the threshing device. The distribution pattern of the threshed and separated mixture is one of the core performance characteristics of the longitudinal axial-flow threshing device (*Cheng et al., 2019*). The distribution characteristics of grains, stalks, broken leaves and other debris in the threshing chamber and sieve surface directly affect the indicators of grain crushing rate, uncleaned rate and carryover loss rate in the threshing process, and are also related to the load distribution, cleaning efficiency and cleaning quality of the subsequent cleaning system (*Fu et al., 2021*).

Scholars at home and abroad had conducted theoretical and experimental research on the characteristics, motion, and distribution patterns of threshed and separated mixtures.

Yuejiang Teng, Lecturer, Ph.D.; Chengqian Jin, Prof., Ph.D.; Fuxiang Xie, Prof., Ph.D.; Jian Song, Prof., Ph.D.

Vlădut et al. (2022) present a mathematical model that characterizes the process of threshing and separation from the threshing machine with an axial flow of a thresher, taking into account the following input parameters: material flow, rotor speed, distance between rotor and counter rotor, mean density of processed material, feed speed, length of thresher and separating surface. Output parameters, such as the distribution function of separated seeds, distribution density function of separated seeds and distribution function of free seeds in the threshing space, as well as the distribution function of unthreshed seeds, together with the value of evacuation losses, were used to control the modeling process. *Yue et al. (2023)* studied the distribution pattern of threshed mixture in a double longitudinal axial flow threshing device. The results showed that as the axial distance of the threshing drum increased, the mass of corn kernels in the threshed mixture first increased and then decreased, while the mass of corn cobs continued to increase. In the radial direction of the drum, the mass of corn kernels and corn stalks is higher in the middle and on both sides, with corn kernels most concentrated in the middle and corn stalks mainly on the sides. *Hu et al. (2024)* researched the influence of the soybean threshing and separation device's working parameters on the distribution and uniformity of the threshed mixture in the axial and radial directions of the drum. The results showed that the mass of the threshed mixture and soybean seeds showed a trend of first rapidly increasing and then slowly decreasing in the axial direction of the drum. Additionally, the mass showed a distribution feature of large values on both sides and small values in the middle in the radial direction. A lower drum speed, greater threshing clearance, and a smaller feeding rate make the radial distribution of a threshed mixture more uniform. *Zhan et al. (2025)* explored the material movement and distribution characteristics inside the threshing drum during rapeseed threshing, and established a simplified DEM model with three typical particle types (seeds, pods, stalks). A simulation system for the internal environment of the threshing drum was constructed, and the material distribution and dynamic movement trajectories were analyzed by combining with high-speed photography experiments. The results indicated that the materials mainly moved in a helical manner along the outer edge of the drum; seeds and pods were predominantly concentrated in Collection Box 2, accounting for 33.6% and 27.6% of the total respectively.

In summary, domestic and foreign scholars have conducted extensive research on the performance optimization of longitudinal flow threshing devices, focusing on the structural design of threshing elements, optimization of working parameters, and threshing damage mechanisms, and have achieved phased results (*Gu et al., 2026; Wang et al., 2022; Zhan et al., 2025*). Foreign research has focused more on quantifying the influencing factors of threshing and optimizing threshing components, but has not fully considered the synergistic effect of threshing components and concave plates on the distribution of extracted materials (*Vlăduț et al., 2023; Guo et al., 2025*). Domestic research has made breakthroughs in biomimetic threshing technology and rigid flexible coupling threshing structures, reducing grain damage by optimizing the arrangement of threshing elements (*Lu et al., 2025; Yuan et al., 2019*). However, related studies have mostly focused on low moisture crop conditions, and there is a lack of systematic exploration of the distribution pattern of the extracted material (*Chan et al., 2020; Li et al., 2022*). There is also no optimization plan for threshing device parameters based on distribution pattern (*Aliev et al., 2018; Cristea et al., 2023*).

Conducting experimental research on the distribution pattern of the detached material in the longitudinal flow threshing device has important theoretical value and engineering practical significance in response to the prominent problems of uneven distribution and low cleaning efficiency in the wheat harvesting process, as well as the shortcomings of existing research (*Li et al., 2025; Mircea et al., 2020; Shu et al., 2022*). This study aims to establish the longitudinal axial-flow threshing device with adjustable threshing force to reveal the inherent patterns of the distribution of the threshed mixture. It provides experimental basis and theoretical support for the structural optimization, working parameter matching, and collaborative design of subsequent cleaning systems of the longitudinal flow threshing device, helping to improve the efficiency and low loss of grain harvesting and promote the development of agricultural harvesting equipment towards higher performance and intelligence.

MATERIALS AND METHODS

Overall structure of threshing device

The structure of the longitudinal axial-flow threshing device with adjustable threshing force is shown in Fig. 1, mainly composed of trapezoidal threshing drum, adjustable-threshing-force concave, 360 ° separation device, and operating parameter adjustment device. The concave plate sieves of the longitudinal axial-flow threshing device with adjustable threshing force were adjustable-threshing-force concave, 360 ° separation concave sieve and grid-type concave sieves from front to back.

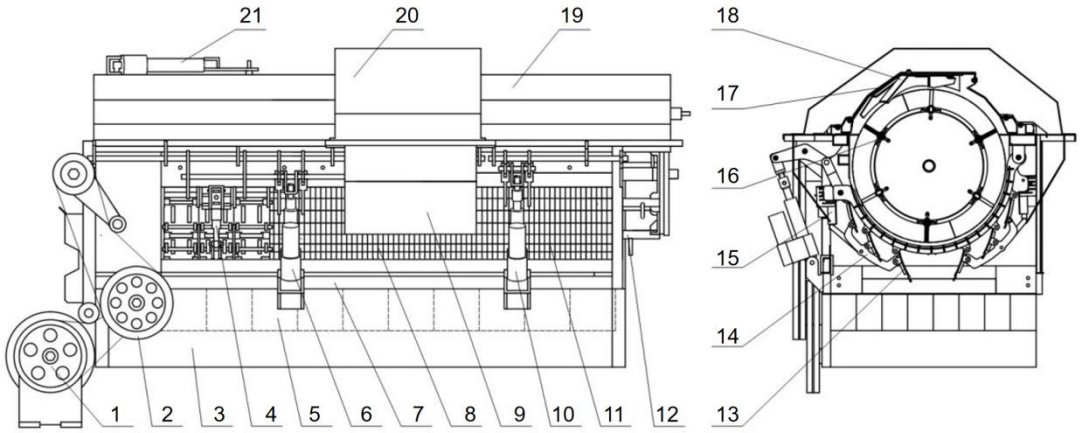

(a) - Right view (b) - Rear view

Fig. 1 - Structural diagram of the longitudinal axial-flow threshing device with adjustable threshing force

1 – hydraulic motor; 2 – drive system; 3 – cleaning chamber frame; 4 – adjustable-threshing-force concave; 5 – material receiving drawer; 6 – electric push rod for gap adjustment of adjustable-threshing-force concave; 7 – threshing chamber frame; 8 – threshing concave sieve; 9 – reflowing plate; 10 – electric push rod for gap adjustment of separating concave sieve; 11 – separating concave sieve; 12 – trapezoid threshing drum; 13 – adjustable plates for threshing force; 14 – transmission mechanism of adjustable plates for threshing force; 15 – electric push rod of adjustable plates for threshing force;16 – threshing rod; 17 – separating plate of 360° separating device; 18 – deflector for material; 19 – top cover ; 20 – 360° separation device; 21 – electric push rod for angle adjustment of deflector for material

The structure of trapezoidal threshing drum and the distribution of material receiving boxes

To prevent the problem of clogging of the threshing drum caused by fluctuations in feeding amount during operation, the structure of trapezoidal threshing drum was adopted in the segmented longitudinal flow threshing device, as shown in Fig.2. The threshing drum was divided into four sections from front to back according to its main functions: feeding section, anti-clogging threshing section, ordinary threshing separation section, and impurity removal section. During the experiment, the threshed and separated mixture was collected by the material receiving drawer installed under the concave plate screen of the threshing device, as shown in Fig. 2. In the material receiving drawer, 8 rows and 10 columns (a total of 80) small material receiving boxes were placed along the axial and radial directions of the drum. The size (length x width) of each material receiving box was 170 mm x 100 mm.

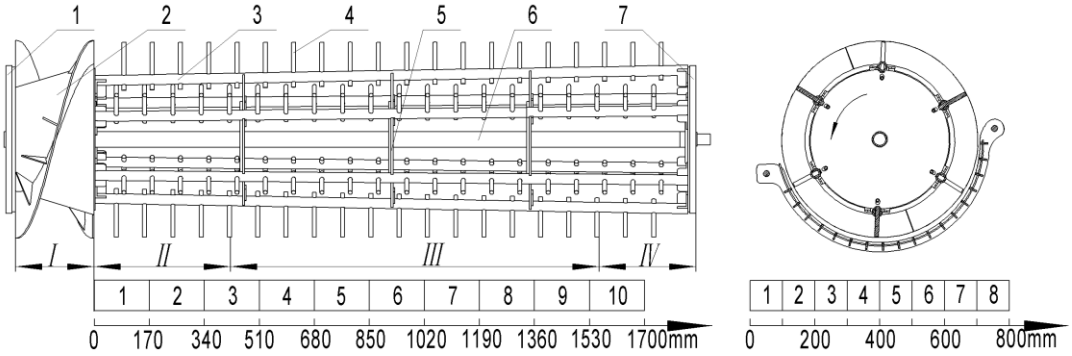

(a) - Structure diagram of trapezoid threshing drum and axial distribution of material receiving boxes

(b) - Structure diagram of radial distribution of material receiving boxes

Fig. 2 - Structure diagram of trapezoid threshing drum and material receiving box distribution

1 - front end cover; 2 - spiral feeding header; 3 - mounting tube for threshing rod; 4 - threshing rod; 5 - intermediate spoke; 6 - spindle ;7 - rear end cover; I - feeding section; II - anti clogging threshing section; III - ordinary threshing separation section; IV - impurity removal section

The structure of adjustable-threshing-force concave

The overall structure of the adjustable-threshing-force concave is shown in Fig. 3, mainly composed of horizontal grid plate, sieve mesh, arc-shaped plate, mounting base for electric push rod, electric push rod, transmission rod and adjustable plate for threshing force. The adjustable threshing force plates were divided into left and right parts, each consisting of 9 boards in 3 rows and 3 columns. Each adjustable plates for threshing force were hinged on one side of the concave sieve frame, and the other side was uniformly controlled by an electric push rod through a transmission mechanism, which could switch state between open mode and closed mode. Both left and right electric push rods were fixed on the concave sieve frame.

The required threshing force varied when threshing different crops or the same crop under different feeding conditions. As shown in Fig. 3, the adjustable threshing force plates could be adjusted to the open mode or closed mode according to different operating conditions to adjust the threshing force.

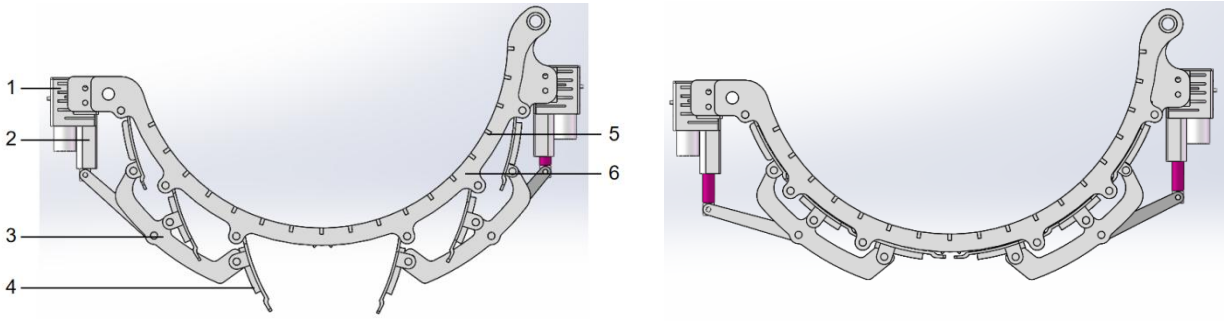

(a) - Open mode (b) - Closed mode

Fig. 3 - Different mode of the adjustable threshing force plates

1 – mounting base for electric push rod; 2 – electric push rod; 3 – transmission rod; 4 – adjustable plates for threshing force; 5 – horizontal partition plate; 6 – arc plate

Test materials

The height of the wheat plant used in the experiment was 670 mm, with the grass to grain ratio of 1:1.28, the grain moisture content of 14.6%, the stem moisture content of 25.3%, and the grain mass of 3.8 g per hundred grains. The experiment was carried out under natural indoor environment with an ambient temperature of 23°C and relative air humidity of 55%. The wheat material was harvested from the experimental field in Hedong District, Linyi City, Shandong Province, with uniform growth and consistent maturity, which could ensure the stability and repeatability of the test results.

Test Method

During the experiment, the operating parameters of the threshing and separating device were set and the threshed and separated mixture below the concave sieve was collected using the material receiving drawer. When analyzing samples, firstly, an electronic balance was used to weigh the total mass of the threshed and separated mixture in each material receiving box. Then, manual sorting was used to separate the materials (grains, chaff, stalks, straw fragments, etc., as shown in Fig. 4) from the material receiving box, and the mass of each component was weighed separately.

(a) - Wheat grains (b) - Wheat chaff (c) - Wheat stalks (d) - Straw fragments

Fig. 4 - The various components of the threshed and separated mixture

Three parallel experiments were conducted under each set of working parameter conditions, and the average of the three experiments was taken as the test result. During the experiment, in order to improve the efficiency of sample analysis, the chaff and straw fragments were combined and counted together, collectively referred to as light impurities.

The calculation method for the mass of light impurities is shown in Equation (1).

$$W_l = W_t - W_g - W_s \quad (1)$$

where:

W_l is the mass of light impurities, g; W_t is the total mass of threshed and separated mixture, g;

W_g is the mass of grains, g; W_s is the mass of stalks, g.

The working parameters of test device

During the experiment, the adjustable-threshing-force concave was adjusted to closed mode. The remaining working parameters of the threshing device were set as follows: drum speed was set to 900 r/min,

guide plate angle was set to 80°, threshing gap was set to 15 mm, separation gap was set to 20 mm, and feeding rate was set to 5 kg/s (*Chan et al., 2020; Gu et al., 2026; Yuan et al., 2019*). The total mass of crops fed into the threshing device corresponding to each experimental parameter was approximately 10 kg. The above working parameters were determined based on preliminary exploratory tests, relevant literature on wheat axial-flow threshing devices, and the receiving capacity of the material receiving drawer. The parameters were set within a reasonable and conventional operating range suitable for wheat threshing, which could ensure stable operation of the test device and meet the requirements of threshing and separation performance tests.

RESULTS AND DISCUSSION

The test results in the closed mode of the adjustable-threshing-force concave are shown in Table 1. In order to understood the distribution pattern of the mixture more intuitively, MATLAB software was use to process the experimental data shown in Table 1, and a three-dimensional schematic diagram of the distribution pattern of the threshed and separated mixture was obtained as shown in Fig. 5.

Table 1

Experimental results of the distribution pattern of the threshed and separated mixture

Mass of threshed and separated mixture [g]								
Radial distance [mm] / Axial distance [mm]	0~100	101~200	201~300	301~400	401~500	501~600	601~700	701~800
0~170	29	27	22	16	14	21	23	25
171~340	79	72	56	47	44	52	70	76
341~510	248	210	189	142	139	177	206	239
511~680	324	268	230	181	178	222	263	313
681~850	284	237	207	162	156	203	237	277
851~1020	238	202	167	136	132	169	194	235
1021~1190	162	134	113	191	89	116	135	161
1191~1360	91	76	68	51	49	63	73	85
1361~1530	44	39	33	25	24	32	35	40
1531~1700	22	20	17	12	12	15	17	21

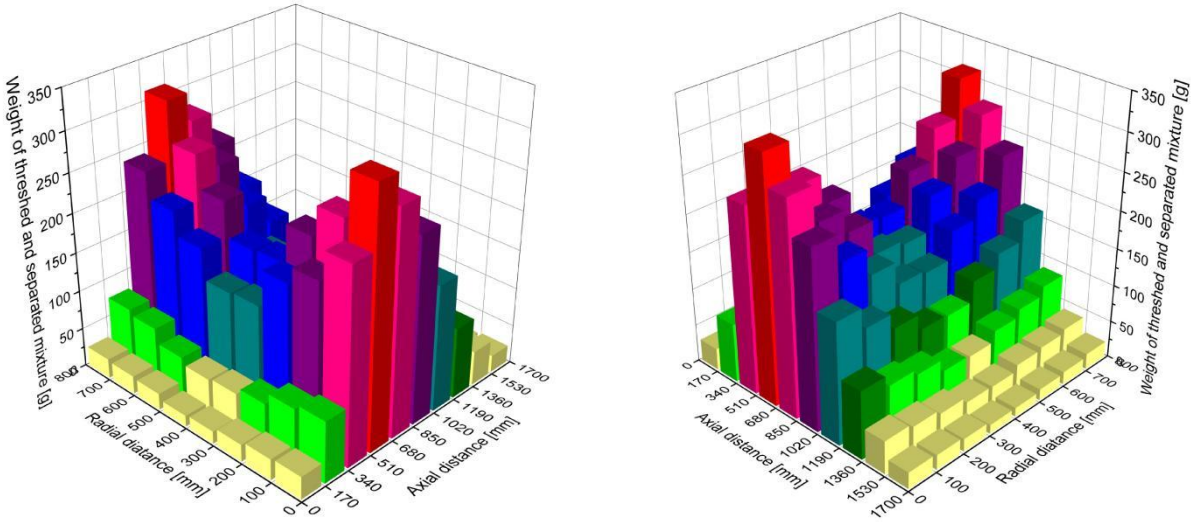

(a) - Left front view (b) - Left rear view

Fig. 5 - Schematic diagram of three-dimensional distribution of threshed and separated mixture in the closed mode of the adjustable-threshing-force concave

According to the data presented in Table 1 and Fig. 5, approximately 9403 g of the threshed and separated mixture passed through the concave sieve, while about 597 g was discharged from the outlet of the threshing drum. This indicates that approximately 94.03% of the feed material passed through the concave sieve and entered the cleaning system. The total mass of the threshed and separated mixture exhibits a characteristic distribution pattern: along the axial direction, it shows enrichment in the middle section and

attenuation at both the inlet and outlet; along the radial direction, the distribution is higher on both sides and slightly lower in the center. The specific distribution characteristics are as follows:

Within the range of 0 ~ 1700 mm along the axial distance of the threshing drum, the mass of the mixture exhibited a parabolic distribution with a low initial stage, a high intermediate stage, and a slow decrease in the remaining stage. Within the range of 0 ~ 340 mm along the axial distance, the mass of the mixture gradually increased from 14 ~ 29 g to 44 ~ 79 g, indicating that the material had just entered the threshing area and was in the initial stage of threshing and separation, with the cumulative amount gradually increasing with transportation.

Meanwhile, due to the adjustable-threshing-force concave being in the closed mode, the threshed mixture could not pass through the concave plate screen directly in this section. As the material continued to flow backwards, in the area without the adjustable threshing force plates, the threshed material passed through the concave sieve. During the falling process, under the action of wind, some of the threshed and separated mixture was blown back to the axial distance of 0 ~ 340 mm for subsequent cleaning treatment. The axial distance range of 341 ~ 850 mm was the peak mass area in the global system, with the 511 ~ 680 mm section reaching the highest value. For example, the mass of the threshed material within the radial distance range of 0 ~ 100 mm in this section was 324 g, and the mass of the threshed material within the radial distance range of 701 ~ 800 mm in this section was 313 g. This was because this area was the main threshing and separation zone of the threshing drum. And the 360° separation device was also located in this area. The retention time of the materials in this area was the longest and the intensity of their separation was the greatest. This area was where the material was most concentrated on the surface of cleaning sieve. Within the axial distance range of 851-1700 mm, the mass of the mixture continuously decreased from its peak value. The mass of the threshed and separated mixture decreased to 49 ~ 91 g in the 1191 ~ 1360 mm range, and further decreased to 12 ~ 22 g in the 1531 ~ 1700 mm range. This indicated that after separation in the core area, residual light impurities and unseparated materials were gradually discharged towards the rear end of the drum, and the remaining materials on the cleaning screen surface were significantly reduced.

In terms of radial distance, the range of 0 ~ 100 mm and 701 ~ 800 mm were the high-value areas for the mass of the threshed and separated mixture. This was due to the coupling effect between the centrifugal force of the threshing drum and the airflow on the surface of cleaning sieve. Under the drive of centrifugal force, the materials migrated to both sides of the drum, while the airflow on the sieve surface lift them up, causing the grains to accumulate in the areas on both sides. Within the radial distance range of 301 ~ 500 mm, the mass of the threshed and separated mixture was only 12 ~ 191 g, which was relatively low. Especially in the end section with the radial distance of 1531 ~ 1700 mm, the minimum mass of the threshed and separated mixture was only 12 g, which was the low value zone of the radial area. This was because the airflow shear force at the center line of the drum was stronger, and the vibration energy was more rapidly attenuated. As a result, the material was more likely to spread to the sides, leading to less retention in the central area.

In order to better analyze the distribution pattern of each component in the threshed and separated mixture, Origin software was used to process the experimental data. The variation patterns of each component in the threshed and separated mixture along the radial direction of the drum were obtained as shown in Fig. 6.

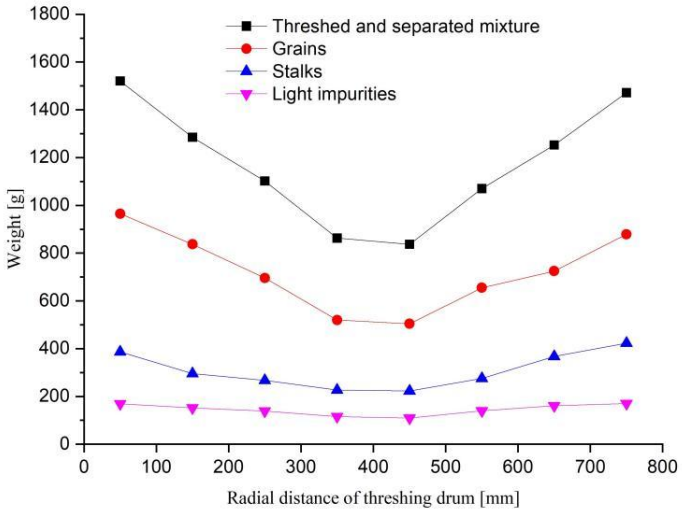

Fig. 6 - Distribution pattern of each component of the threshed and separated mixture along the radial direction of the threshing drum

The mass of the threshed and separated mixture and its components decreased first and then increased with the increase of the radial distance of the threshing drum, and the change curve showed a quadratic distribution with an upward opening. The mass of the threshed and separated mixture followed a U-shaped distribution along the radial direction of the threshing drum, with high at both ends and low at the center. The mass of the threshed and separated mixture in the two end regions (0 mm and 800 mm) was the highest, approximately 1520 g and 1480 g, respectively. The mass of the threshed and separated mixture in the area near the center line (400 ~ 500 mm) was the lowest, about 830 ~ 850 g.

The overall symmetry of the distribution curve was good, reflecting the core pattern of material migration to both sides under the centrifugal force of the threshing drum. The distribution of grains was consistent with the overall trend of the threshed and separated mixture, showing a U-shaped distribution. The mass of the grains at both ends was about 960 g, and the mass near the center line was about 500 g. As shown in the figure, the proportion of grain mass in the mass of the threshed and separated mixture was the highest. The distribution of stalks also followed a U-shaped curve. Its radial variation with the threshing drum was relatively gentle compared to the grain. The stalks mass of the two end areas was about 380 ~ 430 g, and the mass of the area near the center line was about 220 g. The mass proportion of stalks in the threshed and separated mixture was second only to that of grains. The proportion of light impurities was the lowest and the distribution was the most uniform. The mass of the light impurities at both ends was about 160 ~ 170 g, and the mass near the center line is about 100 ~ 110 g. The variation amplitude of the mass of light impurities along the radial direction of the threshing drum was the smallest, which reflected that light impurities was more easily uniformly diffused by the influence of airflow.

The variation pattern of the mass of the threshed and separated mixture along the radial direction of the threshing drum was fitted using MATLAB software. The regression equation was obtained as shown in Equation (2), and the correlation coefficient R^2 of the equation was 0.9449. This regression equation could provide reference and basis for the structural optimization of threshing and separating devices, as well as the structural design and energy allocation of cleaning devices.

$$T_1(x)=4.951\times10^{-3}\times x^2-4.035\times x+1700 \quad (2)$$

where: $T_1(x)$ is the mass of the threshed and separated mixture along the radial direction of the threshing drum, g; x is the radial direction of the threshing drum, mm.

The variation patterns of each component in the threshed and separated mixture along the Axial direction of the drum were obtained as shown in Fig. 7. In the axial direction of the threshing drum, the distribution of the threshing separating mixture first sharply increased, reaching a peak at 510 mm (about 1980 g), and then continued to decrease, reaching about 120 g at 1700 mm.

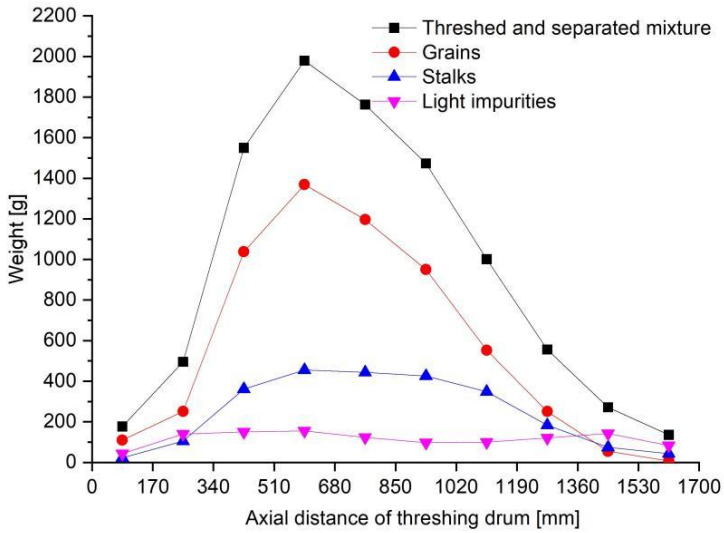

Fig. 7 - Distribution pattern of each component of the threshed and separated mixture along the axial direction of the drum

The distribution characteristics of the threshed and separated mixture showed a clear single peak to the left distribution, that was, the mixture was mainly concentrated in the front section (0 ~ 1020 mm) of the drum, and the mass proportion of the rear section (1190 ~ 1700 mm) was significantly reduced.

Within the axial range of 0 ~ 510 mm of the threshing drum, the mass of the stalks gradually increased, indicating that as the drum advanced, the stalks were gradually broken and separated. Within the range of 510 ~ 1190 mm, the stem mass remained at a relatively high level, indicating a longer duration of stem separation that run through the rear section of the drum. Within the range of 1190-1700 mm, the mass of the stalks slowly decreased, indicating that a small amount of long stalks were still separated in the rear section of the drum. The overall mass of separated stalks was much lower than that of grains. The separation of stalks lagged behind that of grains and was more evenly distributed, which could lead to relatively concentrated stem load in the middle and later stages of the sieve surface.

Within the axial range of 0 ~ 510 mm of the threshing drum, the mass of light impurities slowly increased, indicating that light impurities were separated synchronously with the grains and stalks. Within the range of 510 ~ 1700 mm, the mass of light impurities remained at a stable low level, indicating that there was a small amount of separation of light impurities throughout the entire axial range. The distribution of light impurities reached a small peak of about 150 g at 510 mm, and then stabilized between 80 ~ 150 g with gentle fluctuations. The overall mass of light impurities was the lowest, and its distribution was the most uniform. Grains, stalks, and light impurities accounted for 61.48%, 26.22%, and 12.3% of the total mass of the threshed and separated mixture, respectively. The distribution pattern of the mass of the threshed and separated mixture along the axis direction of the drum was fitted using MATLAB software, and the regression equation was obtained as shown in Equation (3), with a correlation coefficient R^2 of 0.9274. This regression equation could provide reference and basis for the structural optimization of threshing and separating devices, as well as the structural design and energy allocation of cleaning devices.

$$T_2(y)=1.914\times10^{-6}\times y^3-7.344\times10^{-3}\times y^2+7.312\times y-586.9 \quad (3)$$

where: $T_2(y)$ is the mass of the threshed and separated mixture along the axial direction of the threshing drum, g; y is the axial direction of the threshing drum, mm.

The variation of grain breakage rate in the axial direction was analyzed, and the relationship curve between grain breakage rate and axial distance was obtained as shown in Fig. 8. With the increase of axial distance of the threshing drum, the grain breakage rate showed a slow increasing trend (within the range of 0 ~ 1360 mm axial distance), followed by a sharp increasing trend (within the range of 1360 ~ 1700 mm axial distance).

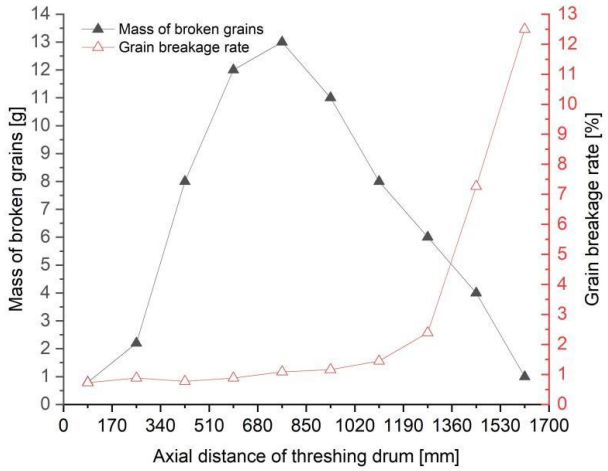

Fig. 8 - Relationship between grain breakage rate and axial distance of the threshing drum

The distribution pattern of grain breakage rate along the axial distance of the threshing drum was fitted using MATLAB software, and the regression equation was obtained as shown in Equation (4), with a correlation coefficient R^2 of 0.987.

$$P_1(y)=3.882\times10^{-9}\times y^3-6.732\times10^{-6}\times y^2+3.101\times10^{-3}\times y+0.361 \quad (4)$$

where:

$P_1(y)$ is the grain breakage rate along the axial distance of the threshing drum, g; y is the axial direction of the threshing drum, mm.

By using Equations (2), (3), and (4), a basis for optimizing the structure and working parameters of the threshing and separation device when the threshing force adjustment plate was in the closed state could be provided, thereby reducing energy consumption and improving the quality of the operation.

Structural optimization

As shown in Fig. 8, the grain breakage rate increased significantly with the increase of axial distance, especially in the range of 1020 ~ 1700 mm, where the grain breakage rate rose rapidly from 1.16% to 12.5%. This indicated that the threshing intensity in this section was excessively high, resulting in serious grain damage. Therefore, targeted structural optimization was carried out based on the distribution law of grain breakage rate. The optimization objective was to reduce the rigid impact and shearing effect of threshing rod teeth on grains, so as to lower the grain breakage rate without reducing threshing performance.

The optimized structure is shown in Fig. 9. The threshing rods in the axial range of 1050 ~ 1690 mm were fully covered with polyurethane rubber sleeves, which could soften the threshing force and buffer the impact on grains.

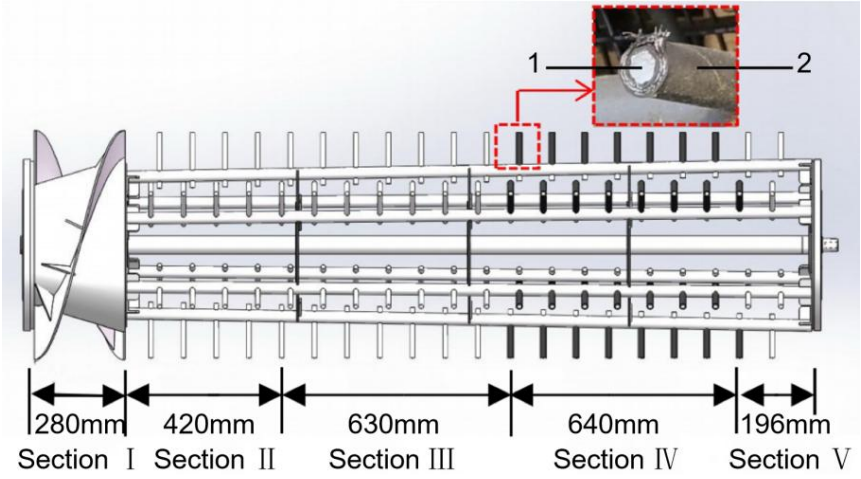

Fig. 9 - Structural diagram of threshing drum after structural optimization

1-Threshing rod teeth; 2 - polyurethane rubber

The threshing test was conducted on the optimized threshing drum under the same operating conditions, and the test result is shown in Fig.10.

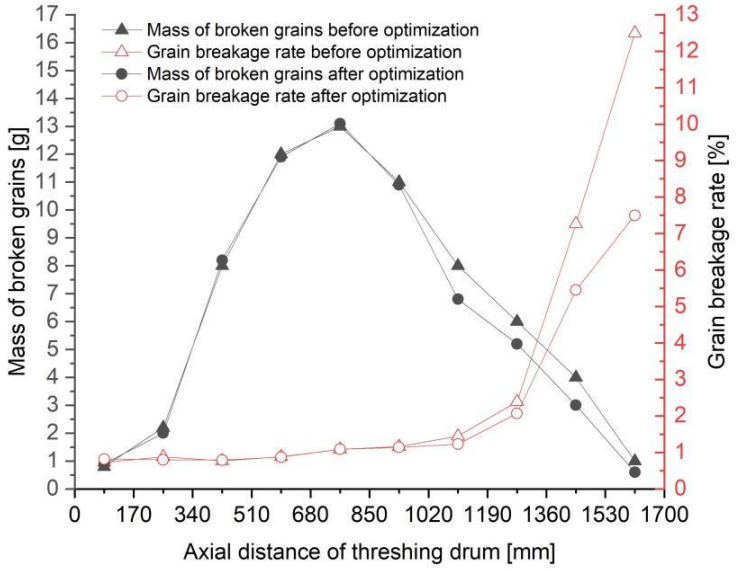

Fig. 10 - Comparison of grain breakage rates before and after structural optimization

As shown in the figure above, within the axial distance range of 0 ~ 1020 mm, the grain breakage rate after structural optimization was not significantly different from that before structural optimization. However, within the axial distance range of 1020 mm ~ 1700 mm from the threshing drum, the grain breakage rate after structural optimization decreased from 1.16% ~ 12.5% to 1.05% ~ 7.5%, which showed a significant reduction compared to the grain breakage rate before structural optimization. This indicated that the structural optimization could effectively reduce the destructive force of the threshing rod teeth on crops in this area, thereby reducing the grain breakage rate.

CONCLUSIONS

1) The experiment investigated the mass distribution characteristics of the threshed and separated mixture along the axial (0~1700 mm) and radial (0~800 mm) directions of the threshing drum. The results indicate that, along the axial direction, the mixture exhibits a left-skewed unimodal distribution, characterized by enrichment in the middle section and attenuation toward both the inlet and outlet. Along the radial direction, a U-shaped distribution is observed, with higher mass at both sides and lower mass at the center. The distribution trends of wheat grains, stalks, and light impurities are consistent with those of the overall mixture, differing primarily in their proportions (61.48%, 26.22%, and 12.30%, respectively) and in the degree of distribution uniformity.

2) The experimental data was processed and fitted, and the regression equations of the mass of the threshed and separated mixture and grain breakage rate along the radial and axial directions of the drum were obtained, with the correlation coefficients R^2 reaching 0.9449, 0.9274 and 0.987 respectively. These equations provide a quantitative reference basis for the structural optimization of threshing and separating devices, as well as the structural design and energy allocation of cleaning devices.

3) Aiming at the problem that the grain breakage rate increased significantly from 1.16% to 12.5% in the axial range of 1020~1700 mm of the drum, structural optimization was carried out by covering the threshing rods in this range with polyurethane rubber sleeves. The threshing test under the same operating conditions showed that the grain breakage rate in the range of 1020 ~1700 mm decreased to 1.05%~7.5% after optimization, with no significant change in the range of 0 ~1020 mm. This optimization effectively reduced the destructive force of the threshing rod teeth on crops in the target area, thus decreasing the grain breakage rate and improving the quality of threshing operation.

ACKNOWLEDGEMENT

This work was supported by Weifang City Science and Technology Development Plan Project (grant numbers 2025GX010) and the doctoral research start-up fee (grant numbers 44122025).

REFERENCES

[1] Aliev, E.B., Yaropud, V.M., Dudin, V.Y., Pryshliak, V.M., Pryshliak, N.V., & Ivlev, V.V., (2018). Research on sunflower seeds separation by airflow. *INMATEH - Agricultural Engineering*, 56(3), 119 - 128.

[2] Chan, Y., Kang, Y., Wang, T., Ning, X., Jin, C., & Yin, X. (2020). Distribution regularities of the threshed mixtures in longitudinal axial flow flexible thresher of soybean harvester (大豆收获机纵轴流柔性脱粒装置脱出物分布规律). *Journal of China Agricultural University*, 25(09), 104-101.

[3] Cheng, C., Fu, J., Chen, Z., & Ren, L. (2019). Effect of vibration parameters of vibrating screen for harvester on adhesion characteristics of threshed mixtures with different moistures (收获机振动筛振动参数影响不同湿度脱出物粘附特性). *Transactions of the Chinese Society of Agricultural Engineering*, 35(8), 29-36.

[4] Cristea, O.D., Niţu, M., Constantin, G., Munteanu, M., Milea, O-E., Zaharia, R., & Grădilă, M., (2023). Research on the testing of axial flow threshing apparatus for improving their qualitative working indices, *INMATEH - Agricultural Engineering,* 70(2), pp. 607-614, DOI: https://doi.org/10.35633/inmateh-70-58.

[5] Fu, J., Xie, G., Ji, C., Wang, W., Zhou, Y., Zhang, G., Zha, X., & Abdeen, M.A. (2021). Study on the distribution pattern of threshed mixture by drum-shape bar-tooth longitudinal axial flow threshing and separating device. *Agriculture*, 11, 756-770.

[6] Gu, T., Qian, P., Tang, Z., & Gu, X., (2026). Effect of wet rice state on threshing process and threshed mixture of combine harvester (水稻潮湿状态对联合收获机脱粒过程及脱出物的影响). *Journal of Agricultural Mechanization Research*, 48(1), 41-47.

[7] Guo, H., Han, J., Lü, Z., Dong, Y., Guo, L., & Zhou, W., (2025). Discrete element model construction and parameter calibration of combined harvest oil sunflower extract (联合收获油葵脱出物离散元模型构建与参数标定). *Transactions of the Chinese Society for Agricultural Machinery*, 56(5), 319-330.

[8] Hu, Y., Tang, Z., Wang, S., Li, B., Guo, X., & Chen, S., (2024). The influence of the distribution law and uniformity of a threshed mixture with the working parameters of a soybean threshing device. *Agronomy*, 14, 1581-1596.

[9] Li, Q., Xie, F., Kang, J., Wang, X., & Luo, Q., (2022). Parameter optimization and experiment on post-threshed mixture for the cleaning device in 4LZ-4.0 combine harvester of soybean (4LZ–4.0 大豆联合收割机清选装置参数优化及脱出物分布试验). *Journal of Hunan Agricultural University (Natural Sciences)*, 48(6), 737-743.

[10] Li, L., Zhou, Y., Nie, J., Li, Q., Zhang, L., (2025). Optimization design of tangential flow-transverse axial flow double drum maize threshing device based on EDEM (基于 EDEM 的切流-横轴流双滚筒玉米脱粒装置的优化). *INMATEH - Agricultural Engineering*, Vol.77, No. 3, 647-662.

[11] Lu, M., Li, Q., Wang, S., Liu, X., & Lü, W., (2025). Vibration sieving simulation of Chinese cabbage seed extracts based on EDEM (基于 EDEM 的大白菜种子脱出物振动筛分模拟研究). *Journal of Agricultural Mechanization Research*, 47(5), 9-14.

[12] Mircea, C., Nenciu, F., Vladut, V., Voicu, G., Gageanu, I., & Cujbescu, D., (2020). Increasing the performance of cylindrical separators for cereal cleaning by using an inner helical coil. *INMATEH - Agricultural Engineering*, 62(3), 249-258.

[13] Shu, C., Yang, J., Wan, X., Yuan, J., Liao, Y., & Liao, Q., (2022). Calibration and experiment of the discrete element simulation parameters of rape threshing mixture in combine harvester (联合收获油菜脱出物离散元仿真参数标定与试验). *Transactions of the Chinese Society of Agricultural Engineering*, Vol. 38, No. 9, 34-43.

[14] Vlădut, N. V., Biriş, S. Ş., Cârdei, P., Găgeanu, I., Cujbescu, D., Ungureanu, N., Popa, L. D., Perişoară, L., Matei, G., & Teliban, G. C., (2022). Contributions to the mathematical modeling of the threshing and separation process in an axial flow combine. *Agriculture*, 12, 1520-1540.

[15] Vlăduț, N. V., Ungureanu, N., Biriş, S. Ş., Voicea, I., Nenciu, F., Găgeanu, I., Cujbescu, D., Popa., L. D., Boruz., S., Matei., G., Ekielski, A., & Teliban, G. C., (2023). Research on the identification of some optimal threshing and separation regimes in the axial flow apparatus. *Agriculture*, 13, 838-854.

[16] Wang, L., Yu, Y., Zhang, S., Song, L., & Feng, X., (2022). Motion characteristics of maize mixture on bionic screen based on earthworm motion characteristics (蚯蚓运动特征仿生筛筛上玉米脱出物运动特性研究). *Transactions of the Chinese Society for Agricultural Machinery*, 55(3), 158-166.

[17] Yuan, J., Wu, C., Li, H., Qi, X., Xiao, X., & Shi, X., (2019). Simulation study on the motion laws of threshed rice through a cylinder sieve (水稻收获脱出物内圆筒筛分运动规律仿真研究). *Journal of Machine Design*, 36(5), 16-24.

[18] Yue, D., Wang, Q., He, Q., Li, D., Yu, Q., Geng, D., & Li, M., (2024). A Study of the Distribution of the threshed mixture by a double longitudinal axial flow corn threshing device. *Agriculture*, 14, 166-178.

[19] Zhan, G., Liu, W., & Zhang, P., (2025). Study on the movement characteristics of rapeseed threshing materials based on dem simulation and high-speed imaging (基于离散元法的谷子脱出物建模与参数标定). *INMATEH - Agricultural Engineering*, Vol.76, No. 2, 1279-1288.

[20] Zhang, D., Huang, Z., Chen, Y., Yi, S., & Li, Y., (2025). Discrete Element Method Based Modeling and Parameter Calibration for Millet Threshing Mixture (基于离散元法的谷子脱出物建模与参数标定). *Transactions of the Chinese Society for Agricultural Machinery*, 56(12), 354-365.